ORIGINAL ARTICLE

The Stability of Fe-Isotope Signatures During Low Salinity Mixing in Subarctic Estuaries

Sarah Conrad[1] · Kathrin Wuttig[2,3] · Nils Jansen[2,4] · Ilia Rodushkin[5] · Johan Ingri[1]

Abstract

We have studied iron (Fe)-isotope signals in particles (> 0.22 μm) and the dissolved phase (< 0.22 μm) in two subarctic, boreal rivers, their estuaries and the adjacent sea in northern Sweden. Both rivers, the Råne and the Kalix, are enriched in Fe and organic carbon (up to 29 μmol/L and up to 730 μmol/L, respectively). Observed changes in the particulate and dissolved phase during spring flood in May suggest different sources of Fe to the rivers during different seasons. While particles show a positive Fe-isotope signal during winter, during spring flood, the values are negative. Increased discharge due to snowmelt in the boreal region is most times accompanied by flushing of the organic-rich sub-surface layers. These upper podzol soil layers have been shown to be a source for Fe-organic carbon aggregates with a negative Fe-isotope signal. During winter, the rivers are mostly fed by deep groundwater, where Fe occurs as Fe(oxy)hydroxides, with a positive Fe-isotope signal. Flocculation during initial estuarine mixing does not change the Fe-isotope compositions of the two phases. Data indicate that the two groups of Fe aggregates flocculate diversely in the estuaries due to differences in their surface structure. Within the open sea, the particulate phase showed heavier δ^{56}Fe values than in the estuaries. Our data indicate the flocculation of the negative Fe-isotope signal in a low salinity environment, due to changes in the ionic strength and further the increase of pH.

Keywords Fe-isotopes · Fe geochemistry · Dissolved and particulate Fe · Organically complexed Fe · Fe(oxy)hydroxides · Salinity gradient · Spring flood

1 Introduction

Despite its high abundance in the continental crust (Wedepohl 1995), Fe can be the limiting element in a third of the ocean surface waters (Martin et al. 1991; Morel and Price 2003). Riverine Fe input is the main source of Fe to the oceanic Fe budget, and estuarine

---

✉ Sarah Conrad
  sarah.conrad@ltu.se

Extended author information available on the last page of the article

mixing controls how much Fe reaches the oceans (Wells et al. 1995; Raiswell and Canfield 2012). Particles and colloids in river water (ranging from 0.01 to 1 μm) flocculate into larger particles and aggregates due to the increased ionic strength within estuaries and then precipitate close to the shoreline (Boyle et al. 1977; Sholkovitz et al. 1978). These Fe particles and colloids consist mainly of two forms, Fe-rich organic carbon (OC) compounds and Fe-rich (oxy)hydroxides (Ingri et al. 2006; Ilina et al. 2013; Kritzberg et al. 2014). The surface properties of these compounds vary as aggregates with OC have fewer mineral phases exposed at their surface (Eusterhues et al. 2008). The amount of mineral phases, in turn, affects their chemical reactivity during estuarine mixing, which for example is defined by size and speciation (Poulton and Raiswell 2005; Tagliabue et al. 2017). Hence, the river input of Fe into the ocean is substantially modified by flocculation processes that occur at the estuarine interface and dependent on the initial Fe phase (Eckert and Sholkovitz 1976; Boyle et al. 1977; Sholkovitz 1978). Various studies showed the ability of OC to keep Fe in solution along the salinity gradient of an estuary (Krachler et al. 2010; Kritzberg et al. 2014). The aggregation, sedimentation and resulting burial of OC associated with Fe in estuarine environments have been described as the "rusty carbon sink" (Lalonde et al. 2012; Shields et al. 2016).

Earlier studies have addressed the possibility of using Fe-isotopes as a tool to identify water sources and to differentiate between Fe phases, i.e. Fe–OC complexes and Fe(oxy) hydroxides (Ingri et al. 2006; Escoube et al. 2009; Ilina et al. 2013; Poitrasson et al. 2014). In low-temperature environments, stable Fe-isotope mass varies about 6.0–8.0‰ in $^{56}Fe/^{54}Fe$ ratios (Dauphas et al. 2017; Wu et al. 2018), expressed as $\delta^{56}Fe$ relative to the reference material IRMM-14 (Dauphas and Rouxel 2006; Rouxel and Auro 2010). The Fe-isotope values of Fe phases entering the ocean via rivers range between −1.2 and +1.8‰ (Conrad 2019 and references therein), and this variation has been used as a tool to map the contribution of Fe sources to the ocean on temporal and geographical scales (Conway and John 2015). For example, subarctic and temperate rivers supply Fe phases with a negative $\delta^{56}Fe$ value to seawater (Ingri et al. 2006; Severmann et al. 2006; Escoube et al. 2009; Ilina et al. 2013). It has been shown that Fe-isotope fractionation strongly depends on redox reactions (Wiederhold et al. 2006) and the fractionation can be used to trace the Fe-isotope composition of different Fe phases at their origin (Ingri et al. 2006; Ilina et al. 2013; Dos Santos Pinheiro et al. 2014; Poitrasson et al. 2014). In arctic and subarctic rivers, filtration yields towards a separation of a heavy dissolved ($\delta^{56}Fe$ of +0.43‰ ± 0.04‰) and a particulate $\delta^{56}Fe$ between −0.09 and +0.10‰ (Escoube et al. 2009).

In spite of their importance, the knowledge about the fate of different Fe aggregates during estuarine transport is small. The Fe-isotope composition of the Fe-OC aggregates has the potential to be used as a tracer for the cycling of Fe-OC aggregates during transport from land to the open ocean.

Over the last decades, Fe concentrations in boreal rivers draining into the Baltic Sea have been increasing continuously (Kritzberg and Ekström 2012; Sarkkola et al. 2013). Changing redox conditions in organic-rich soils are most likely responsible for the elevated Fe concentrations (Kritzberg and Ekström 2012; Knorr 2013). Higher Fe concentrations lead to increasing coastal export and may have important implications for the receiving aquatic systems.

In this study, we combine the Fe-isotope data from the river mouth, estuary and open sea in a subarctic, boreal environment, to access which Fe phase is present at the varying locations. We show the seasonal variation of dissolved and particulate Fe-isotope ratios in two boreal rivers and their estuaries. Our study provides further information on the seasonal availability of different Fe complexes by the use of their Fe-isotope composition. The

hypothesis was, can the Fe-isotope ratio be used to trace different Fe complexes from the river mouths into the open ocean. Therefore, we address the following research questions: (1) quantify the variation of Fe-isotope values at the river mouths and along their estuaries; (2) identify processes leading to temporal changes; and (3) reveal the effect of salinity-induced mixing on the Fe-isotope ratio.

2 Materials and Methods

2.1 Sampling Site

For this study, water samples were collected in two rivers, their estuaries, and the adjacent sea in Northern Sweden (Fig. 1). The boreal rivers Kalix and Råne have their origin in the Caledonian Mountains and the Råne Träsk, respectively. Both river catchments consist of forest, wetlands and lakes (Online resources ESM_1; SMHI 2018). The main difference is the size of their catchment with the Kalix's being approximately seven times larger than the Råne's catchment. Additionally, the catchment of the Kalix River contains about 11% mountainous area. Both rivers drain into the northernmost part of the Baltic Sea, the so-called Bothnian Bay (Fig. 1b). The Råne estuary is a semi-closed water-body, partly isolated by several islands. The Kalix estuary is more open to the Bothnian Bay and is a so-called salt wedge estuary (Holliday and Liss 1976), where freshwater floats on top of the denser seawater, with the freshwater layer getting thinner towards the sea. The Bothnian Bay and its catchment area (including the Kalix and Råne River) are ice-covered up to 6 months per year (Vihma and Haapala 2009). The catchment area is about 260,700 km^2,
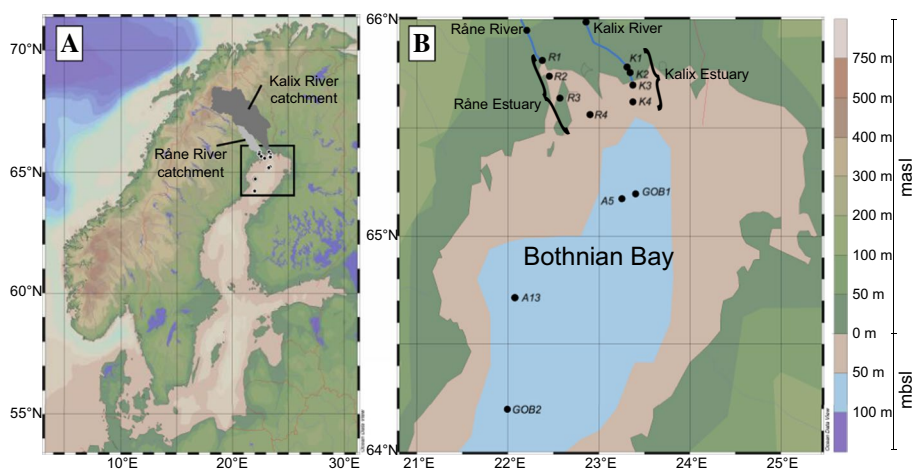

Fig. 1 **A** Overview map of Scandinavia and the Baltic Sea. The black dots display the sampling locations from five different sampling campaigns in Northern Sweden in 2013, 2014 and 2016. The dark and light grey areas mark the geographical locations of the Kalix and Råne River catchments, repectively. **B** Detailed map of the Bothnian Bay, with the sampling locations and their annotations. The two rivers Kalix (K1–4) and Råne (R1–4) drain into the Bothnian Bay (GOB1, GOB2, A5 and A13). Each station was sampled at three depths (0.5 m, 5 m and 10 m) if station depths allowed it. The legend on the right side of the maps shows metre above and below sea level (masl and mbsl, respectively). The Ocean Data View program, version 4.7.10 was used to generate the maps (Schlitzer, R., Ocean Data View, http://odv.awi.de, 2018)

and the high freshwater input and the low tide-influence lead to salinities below 4 (Kautsky and Kautsky 2000).

The boreal region has a subarctic climate, with extreme seasonal temperature variations, with long, cold winters (−20 to −40 °C) and short, mild summers (20–30 °C), (Peel et al. 2007). Between 40 and 50% of the precipitation is snow (Ingri et al. 2005). With 5–7 months of winter, the moisture in the soils and subsoils freezes between 25 and 79 cm deep (Öquist and Laudon 2008; Haei et al. 2010). The river discharge has significant seasonal variations, and the main hydrological event is occurring in spring due to snow and ice melt (Fig. 2). There is an extended period of high discharge in the Kalix River, compared to the Råne River, resulting from snow and ice melt in mountainous regions (Fig. 2). Discharge for both rivers was measured about 50 and 25 km upstream, respectively, at the stations Räktfors (Kalix River) and Niemisel (Råne River) by the Swedish Meteorological and Hydrological Institute (SMHI 2018).

For this study, the rivers, their estuaries and the Bothnian Bay were sampled during pre-flood, spring flood and post-flood (Table 1). Pre-flood samples were collected from beneath the ice-covered estuaries, in March 2014. Spring flood samples were collected in the estuaries and the Bothnian Bay in May and June 2013. Post-flood samples were collected in the Råne estuary and the Bothnian Bay in July 2014. In addition, pre-flood, spring flood and post-flood in Kalix and Råne River were sampled close to their river mouths between March and June 2016. The coordinates of each sampling location are summarized in the online resources (ESM_1).

2.2 Sampling and sample processing

All sampling stations were sampled at depths of 0.5, 5 and 10 m if they were deep enough (all except station K1 and R1). Water samples from the Kalix estuary, the Råne estuary and the Bothnian Bay were collected from the coast guard vessel KBV005 in May and June 2013. Four stations in each estuary (R1–R4 and K1–K4) and two stations in the Bothnian Bay (A5 and A13) were sampled. During the sampling in March 2014, samples were
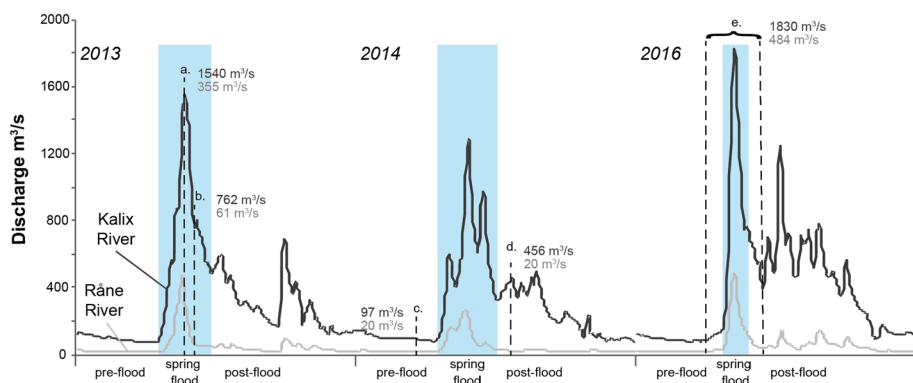

Fig. 2 Discharge from the Kalix (black) and Råne River (grey) during the sampling periods in 2013, 2014 and 2016 (SMHI). The dashed lines and letters indicate the five sampling events (a: 21–23 May 2013, b: 5–7 June 2013, c: 18 and 19 March 2014, d: 21 July 2014, and e: 25 March–15 June 2016). The discharge during each sampling is noted (for sampling event e, the maximum discharge during sampling is noted). Below the *x* axis pre-flood, spring flood and post-flood are denoted for each year and the blue shaded areas mark the different spring flood events

Table 1 Sampling stations and their sampling occasions

	Station	Estuaries and Bothnian Bay				Rivers		
		Spring flood		Pre-flood	Post-flood	Pre-flood	Spring flood	Post-flood
		May 2013	Jun 2013	Mar 2014	Jul 2014	Mar–Jun 2016		
Råne Estuary	R1	R1a	R1b	R1c	–	–	–	–
	R2	R2a	R2b	R2c	R2d	–	–	–
	R3	R3a	R3b	R3c	–	–	–	–
	R4	–	R4b	–	–	–	–	–
Kalix Estuary	K1	K1a	K1b	K1c	–	–	–	–
	K2	K2a	K2b	K2c	–	–	–	–
	K3	K3a	K3b	K3c	–	–	–	–
	K4	K4a	K4b	–	–	–	–	–
Bothian Bay	A5	A5a	A5b	–	–	–	–	–
	A13	A13a	A13b	–	–	–	–	–
	GOB1	–	–	–	GOB1d	–	–	–
	GOB2	–	–	–	GOB2d	–	–	–
Råne River	RR	–	–	–	–	RR1e–RR3e	RR4e–RR9e	RR10e–RR13e
Kalix River	KR	–	–	–	–	KR1e–KR3e	KR4e–KR9e	KR10e–KR13e

The sample notations are assembled by the station name and the sampling event (a: May 2013; b: June 2013; c: March 2014; d: July 2014; e: March to June 2016). Information on the flow environment can be found for each sampling

obtained from the first three stations in the estuaries (R1–R3 and K1–K3), which were ice-covered. Details on the sampling in May and June 2013 and March 2014 can be found in Bauer et al. (2018). Briefly, the samples in 2013 were collected from the coast guard vessel KBV005 with 2×2 L Niskin bottles (Hydros-Bios, Kiel, Germany which had been custom-made trace metal clean containing only Ti screws, on a Dyneema rope, acid-cleaned 2-L LDPE bottles all parts acid cleaned) on a line in depths of 0.5, 5 and 10 m. In 2014, the samples were conducted through a hole in the ice, drilled with an ice auger and pumped up from the depths of 0.5, 5 and 10 m. During July 2014, the Råne estuary (R2) and two stations in the Bothnian Bay (GOB1 and GOB2) were sampled from the M/S Fyrbyggaren following the procedures and methods by (Cutter et al. 2010). Water samples were obtained with 5-L Niskin bottles (Hydros-Bios, Kiel, Germany) on a line in depths of 0.5, 5 and 10 m. Once retrieved, the bottles were emptied into sample acid-cleaned LDPE bottles, wrapped in polyethylene bags. Salinity, temperature, pH, alkalinity and dissolved oxygen were monitored with a Hydrolab Multisonde 5 (Online resources ESM_1). The sampling stations in the Kalix River, Kamlunge, and in the Råne River, Orrbyn, were partly ice-covered until early May 2016. Samples were collected from a bridge in the middle of each river. Specific conductivity, temperature, pH and dissolved oxygen were monitored with a Hydrolab Multisonde 5 (Online resources ESM_1).

All materials in contact with samples consisted of LDPE and were acid cleaned (1.1 M HNO_3; Merck Millipore pro analysis EMSURE), before and between samplings (Ödman et al. 1999). All water samples were filtered within 6 h through 0.22 -μm pore

size membrane filters (Merck MF-Millipore Membrane Filter, mixed cellulose esters, hydrophilic, diameter 142 mm), which were locked in polycarbonate filter holders under a clean bench with a peristaltic pump, yielding into a particulate (PFe > 0.22 μm) and a dissolved (DFe < 0.22 μm) fraction. Membrane filters were cleaned with ultrapure acetic acid (99–100%) and stored in Milli-Q ultrapure water (18.2 MΩ cm at 25 °C) before they were used. The filtered water was acidified with ultrapure distilled 10% HNO_3 to a pH below 2 and stored at 4 °C. The filters were stored in petri dishes at −18 °C until analyses.

Furthermore, water samples from 2016 were filtered through 0.7-μm glass fibre filters (GF/F Whatman®) for dissolved and particulate organic carbon analyses (DOC and POC). The filters were pre-combusted for four hours to limit the C blanks (Brodie et al. 2011). The filters for POC analyses were stored at −18 °C before analyses by UC Davis Stable Isotope Facility (USA).

3 Analytical Methods

All samples were analysed for elemental composition and Fe-isotope composition in collaboration with ALS (Australian Laboratory Services) Scandinavia AB, Luleå, Sweden. All sample manipulations were performed in a clean laboratory (Class 10,000) by personnel wearing clean room gear and following all general precautions to reduce contamination (Rodushkin et al. 2010). High-purity Suprapure® acids were used throughout sample treatment and analyses. Accredited DOC analyses were determined at the Umeå Marine Sciences Centre (Samples 2013 and 2014) and ALS Scandinavia (Samples 2016).

3.1 Element Concentration by Inductively Coupled Plasma Sector Field Mass Spectrometry (ICP-SFMS)

For the elemental composition, the dissolved samples were diluted (2–200 fold) in 2.2 M HNO_3; the degree of dilution depended on the salinity of the sample. The filters were treated with 10 mL of a 1000:1 mixture of HNO_3/HF overnight followed by closed-vessel digestion in a microwave oven (600 W, 1 h). An aliquot of the digests was further diluted in 2.2.M HNO_3 by the factors of 5 and 50 (2016 and 2013/2014, respectively) for the determination of Fe concentrations.

Multi-elemental analyses (i.a. Fe, Rb, Sr) were performed in the dissolved and particulate phases of the samples by ICP-SFMS (ELEMENT XR, Thermo Scientific, Bremen, Germany). A combination of internal standardization (indium added at 2 μgL^{-1} to all measurement solutions) and external calibration verified the measurements. All measured data fall within a 4-point calibration curve. Details of the analytical procedure as well as instrument parameters and analysis conditions can be found elsewhere (Rodushkin and Ruth 1997; Rodushkin et al. 2005). The analytical procedure was validated with SLRS-4 River Water CRM for Trace Metals, SLEW-2 Estuarine Water CRM for Trace Metals and NASS-4 open ocean water (supplied by National Research Council, Ottawa, Canada), (Rodushkin et al. 2005, 2016). Fe was analysed on three different instrument runs with an average detection limit (LOD) of 14 nM for the dissolved samples and 21 nM for the particulate samples taken in 2013 and 2014 (LOD = X_{bl} + 3SD_{bl}, X_{bl} = mean concentration of Fe in blanks; SD_{bl} = Standard deviation of blanks). Replicated measurements showed a precision of ± 1.3% (n = 8) for the particulate phase and ± 3.0% (n = 3) for the dissolved phase.

Table 2 Iron concentrations and Fe-isotope data for samples taken in the Kalix and the Råne estuary and the Bothnian Bay in 2013 and 2014

Råne Estuary

Sample	Depth (m)	DFe (μM)	Dδ56Fe (‰)	2SD (‰)	PFe (μM)	Pδ56Fe (‰)	2SD (‰)
R1a	0.5	16.26	0.484	0.071	4.51	−0.028	0.035
R1a	5.0	15.33	0.325	0.030	6.49	−0.044	0.018
R2a	0.5	10.76	0.442	0.058	2.26	−0.053	0.034
R2a	5.0	10.33	0.400	0.028	3.49	−0.024	0.038
R2a	10.0	4.66	0.387	0.040	1.71	−0.069	0.062
R3a	0.5	7.11	0.329	0.068	2.78	−0.020	0.008
R3a	5.0	7.05	0.340	0.066	1.80	−0.057	0.050
R3a	10.0	1.72	0.318	0.128	0.42	−0.065	0.052
R1b	0.5	14.04	0.387	0.042	15.49	−0.044	0.062
R1b	5.0	13.54	0.366	0.050	12.23	−0.030	0.032
R2b	0.5	7.07	0.487	0.094	2.26	0.065	0.024
R2b	5.0	7.16	0.414	0.058	2.36	0.062	0.062
R2b	10.0	6.36	0.435	0.022	2.58	0.091	0.046
R3b	0.5	7.27	0.399	0.030	3.82	0.002	0.026
R3b	5.0	7.18	0.434	0.048	2.37	−0.015	0.050
R3b	10.0	6.73	0.390	0.036	2.20	−0.011	0.006
R4b	0.5	9.08	0.469	0.048	3.82	−0.025	0.048
R4b	5.0	9.02	0.488	0.044	3.31	−0.035	0.040
R4b	10.0	7.25	0.490	0.044	3.07	−0.022	0.030
R1c	0.5	8.65	–	–	13.32	0.081	0.058
R1c	5.0	0.91	–	–	0.80	0.071	0.046
R2c	0.5	3.90	–	–	3.22	0.122	0.054
R2c	5.0	1.28	–	–	0.73	0.049	0.072
R2c	10.0	0.50	–	–	0.46	0.021	0.050
R3c	0.5	3.67	–	–	2.52	0.098	0.052
R3c	5.0	1.03	–	–	0.95	0.141	0.054
R3c	10.0	0.52	–	–	0.54	0.048	0.048

Kalix Estuary

Sample	Depth (m)	DFe (μM)	Dδ56Fe (‰)	2SD (‰)	PFe (μM)	δ56PFe (‰)	2SD (‰)
K1a	0.5	17.30	0.420	0.059	4.07	−0.123	0.039
K1a	5.0	16.55	0.371	0.062	2.75	−0.086	0.053
K2a	0.5	16.49	0.436	0.032	4.31	−0.079	0.040
K2a	5.0	18.68	0.411	0.040	5.82	−0.083	0.042
K2a	10.0	17.92	0.411	0.043	4.04	−0.085	0.028
K3a	0.5	17.17	0.449	0.047	5.79	−0.021	0.022
K3a	5.0	16.63	0.454	0.038	4.11	−0.096	0.048
K3a	10.0	11.91	0.425	0.082	2.84	−0.127	0.038
K4a	0.5	5.69	0.412	0.066	0.37	−0.077	0.034
K4a	5.0	5.68	0.426	0.058	2.04	−0.108	0.028
K4a	10.0	5.00	0.403	0.050	1.61	−0.084	0.046
K1b	0.5	8.49	0.220	0.048	4.33	−0.127	0.094
K1b	5.0	1.88	0.314	0.076	1.52	−0.035	0.042
K2b	0.5	8.63	0.276	0.052	4.00	−0.111	0.046
K2b	5.0	5.59	0.338	0.032	3.12	−0.071	0.008
K2b	10.0	1.29	0.321	0.236	1.16	−0.086	0.034
K3b	0.5	8.24	0.449	0.046	4.49	−0.123	0.054
K3b	5.0	10.51	0.399	0.054	4.01	−0.071	0.048
K3b	10.0	1.33	0.156	0.044	0.97	−0.108	0.028
K4b	0.5	8.27	0.484	0.032	1.95	0.015	0.086
K4b	5.0	6.34	0.481	0.030	2.91	−0.056	0.036
K4b	10.0	1.40	0.108	0.070	1.10	−0.124	0.032
K1c	0.5	13.29	–	–	10.39	0.197	0.050
K1c	5.0	2.69	–	–	1.55	−0.015	0.058
K2c	0.5	10.46	–	–	11.38	0.174	0.050
K2c	5.0	2.33	–	–	1.37	−0.050	0.052
K2c	10.0	0.83	–	–	0.55	−0.049	0.062

Bothnian Bay

Sample	Depth (m)	DFe (μM)	Dδ56Fe (‰)	2SD (‰)	PFe (μM)	δ56PFe (‰)	2SD (‰)
A5a	0.5	0.26	–	–	0.35	0.120	0.062
A5a	5.0	0.28	–	–	0.30	0.091	0.064
A5a	10.0	0.28	–	–	0.34	0.105	0.072
A13a	0.5	0.22	–	–	0.29	0.087	0.074
A13a	5.0	0.20	–	–	0.16	0.081	0.040
A13a	10.0	0.19	–	–	0.12	0.078	0.042
A5b	0.5	0.75	–	–	0.66	0.046	0.028
A5b	5.0	0.79	–	–	0.61	0.102	0.006
A5b	10.0	0.62	–	–	0.57	0.086	0.016
A13b	0.5	0.10	–	–	0.22	−0.095	0.066
A13b	5.0	0.10	–	–	0.19	0.055	0.028
A13b	10.0	0.10	–	–	0.18	0.054	0.028
GOB1d	0.5	0.20	–	–	0.18	0.671	0.154
GOB1d	5.0	0.14	–	–	0.32	0.489	0.110
GOB1d	10.0	0.25	–	–	0.28	0.608	0.068
GOB2d	0.5	0.04	–	–	0.31	0.549	0.058
GOB2d	5.0	0.05	–	–	0.14	0.583	0.094
GOB2d	10.0	0.11	–	–	0.20	0.533	0.086

Table 2 (continued)

Råne Estuary

Sample	Depth (m)	DFe (μM)	Dδ56Fe (‰)	2SD (‰)	PFe (μM)	Pδ56Fe (‰)	2SD (‰)
R2d	0.5	0.15	–	–	0.65	0.316	0.062
R2d	5.0	0.22	–	–	0.85	0.378	0.066
R2d	10.0	0.34	–	–	0.53	0.358	0.068

Kalix Estuary

Sample	Depth (m)	DFe (μM)	Dδ56Fe (‰)	2SD (‰)	PFe (μM)	δ56PFe (‰)	2SD (‰)
K3c	0.5	10.74	–	–	11.42	0.209	0.072
K3c	5.0	2.06	–	–	1.43	–0.092	0.090
K3c	10.0	0.73	–	–	0.70	0.261	0.118

Bothnian Bay

Sample	Depth (m)	DFe (μM)	Dδ56Fe (‰)	2SD (‰)	PFe (μM)	δ56PFe (‰)	2SD (‰)

Table 3 Iron concentrations and Fe-isotope data for the Kalix and the Råne River sampled in 2016

	DFe (μM)	Dδ ^{56}Fe (‰)	2σ (‰)	PFe (μM)	Pδ^{56}Fe (‰)	2σ (‰)
Kalix River						
KR2e	8.0	0.587	0.048	6.6	0.239	0.104
KR4e	9.0	0.483	0.050	8.9	0.149	0.052
KR5e	13.4	0.472	0.132	8.1	0.004	0.128
KR6e	13.5	0.472	0.102	11.2	−0.025	0.132
KR7e	11.6	0.494	0.050	11.0	−0.018	0.050
KR9e	6.7	0.576	0.050	5.0	−0.064	0.080
KR10e	6.5	0.496	0.098	4.6	−0.059	0.114
KR13e	5.1	0.521	0.060	4.3	0.068	0.080
Råne River						
RR2e	11.3	0.615	0.044	13.1	0.302	0.058
RR4e	14.1	0.543	0.048	14.1	0.227	0.064
RR5e	14.2	0.549	0.082	12.2	0.127	0.070
RR6e	13.3	0.551	0.076	20.3	0.190	0.058
RR7e	11.0	0.545	0.104	18.4	0.047	0.096
RR9e	9.4	0.589	0.050	11.7	0.017	0.056
RR10e	7.6	0.589	0.044	9.0	−0.072	0.152
RR13e	7.2	0.477	0.048	7.9	−0.012	0.096

The average detection limit for both phases in 2016 was 9 nM and replicated measurements showed a precision of $\pm 4.5\%$ ($n = 41$).

3.2 Iron Isotope Ratio Measurements by MC-ICP-MS

For the Fe-isotope measurements, an aliquot of the dissolved samples and the digested filters was evaporated. Depending on the Fe concentration, 50 and 1000 ml of sample solution was evaporated. The residuals were re-dissolved in 1 mL 8 M HCl. Iron was separated from the matrix elements by using an AG-MP-1 M ion-exchange resin (microporous, 100–200 mm dry mesh size, 75–150 mm wet bead size, Bio-Rad Laboratories AB, Solna, Sweden). After the sample was loaded, the matrix was washed with 9.6 M HCl, and Cu was eluted with 8 ml 5 M Cl. Afterwards, Fe was eluted with 6 ml 2 M HCl and could be used for further steps (Rodushkin et al. 2016). After evaporating to dryness, 50 μL of concentrated HNO_3 was pipetted directly to the residue followed by the addition of 5 mL MQ-water. Samples with high Fe content were diluted with 0.2 M HNO_3 to a concentration of 2 mg L^{-1} in the measurement solutions. Low Fe concentration water samples were further diluted to 0.7–0.9 μmol/L and measured using high-efficiency desolvation nebulizer (Aridus) in a separate analytical sequence. Iron was separated from the matrix by this ion exchange with a yield of > 95%.

Fe-isotope ratio measurements were performed on a multi-collector inductively coupled plasma mass spectrometer (MC-ICP-MS, NEPTUNE and NEPTUNE PLUS) in high-resolution static mode relative to IRMM-14 CRM. The ^{54}(Fe and Cr), ^{56}Fe, ^{57}Fe, ^{58}(Fe and Ni), ^{60}Ni and ^{62}Ni were collected by the eight adjustable Faraday cups of the NEPTUNE. The instruments were equipped with a micro-concentric nebulizer and tandem cyclonic/Scott

double-pass spray chamber. Instrumental mass biases were corrected by sample-standard bracketing using IRMM-14 CRM, while an internal standard (Ni) was added to all samples and used to correct for instrumental drift. The online data correction considered baseline subtraction (120 s before each measurement), calculation of ion beam intensity ratios and filtering of outliers by a 2σ test. Detailed information on the correction procedures can be found in Baxter et al. (2006).

Iron isotope data are expressed as δ^{56}Fe, relative to the IRMM-14 standard.

$$\delta^{56}\text{Fe}(‰) = \left[\frac{\left(^{56}\text{Fe}/^{56}\text{Fe}\right)_{\text{sample}}}{\left(^{56}\text{Fe}/^{56}\text{Fe}\right)_{\text{IRMM-14}}} - 1 \right] * 10^3$$

In-house quality control samples (prepared by sequential dilutions of SPECTROSCAN 10,000 mg L^{-1} Fe element standard for atomic spectroscopy from TEKNOLAB, Drøbak, Norway) were analysed at the beginning and the end of each analytical session to ensure internal consistency of the analytical results. Each analysis was made as a sequence of standard, three samples, standard. All samples and standards were analysed in duplicates, and the internal analytical precision was better than $\pm 0.01\%$ [± 2 standard deviations (SD)].

Fe-isotope ratios in this material were measured on a regular basis at ALS laboratory from 2003, and a mean δ^{56}Fe of -0.24 ± 0.03 ‰ ($n > 120$, one sigma) makes it a suitable reproducibility control for Fe-isotope ratio measurements in low fractionated samples (Baxter et al. 2006). Within the analysed samples, the δ^{56}Fe values were reproduced with a standard deviation of 8.03% for the particulate phase and 2.50% for the dissolved phase in 2013/2014. In 2016, iron isotope data in both phases were reproduced with a precision of 2.7%. In the three-isotope plot of δ^{56}Fe and δ^{57}Fe, all samples plot on a single-mass fractionation line similar to the theoretical kinetic fractionation line (Young et al. 2002; Kavner et al. 2005), which shows the robustness of the measurements (Online resources ESM_2). In this study, we only discuss the δ^{56}Fe, δ^{57}Fe data which are reported in the online resources (ESM_1) including their errors (2SD).

4 Results

4.1 Spring Flood

The peak discharge in the Kalix River was about 3–4 times higher than in the Råne River (Fig. 2). The pH in the Kalix and the Råne River varied between 5.6 and 6.9 with no clear correlation to the discharge (ESM_2, Fig. S2). Within the estuaries, the pH was increasing with distance to the shoreline in both estuaries and showed little variation with depths (from 6.5 to 7.4). pH in the Bothnian Bay showed little variation between 7.7 and 7.9 (ESM_2, Figs. S3 to S5).

The salinity generally increased with distance to the shore and with depths (ESM_2, Fig. S3 to S5). The salinity at the northernmost station (A5) was about 0.5 points lower than at station A13 during late spring flood (2.5 and 2.9, respectively).

The DOC and POC concentrations in both rivers increased with increasing discharge (ESM_2, Fig. S2). DOC concentration ranged from 500 to 740 µmol/L, while POC ranged from 71 to 134 µmol/L. The high DOC concentrations were also found in the estuaries. Overall, the DOC concentration decreased with distance to the shore, and the variations

with depths were negligible (411–718 µmol/L) (ESM_2, Fg S3 and S4). In the Kalix estuary, during spring flood, the DOC concentration increased with distance to the shore (K1–K3) and then decreased towards station K4. During late spring flood, in the Kalix estuary, there is an overall increase towards the sea. In the Råne estuary, the DOC concentration was decreasing from land to sea (ESM_2, Fig. S4). The DOC concentration in the Bothnian Bay was homogenous between 348 and 396 µmol/L. Station A5 had the highest DOC concentrations within the Bothnian Bay during late spring flood (ESM_2, Fig. S5).

Both rivers showed a large increase in DFe and PFe concentration during the spring flood (Fig. 3; Table 2). The main increase in DFe occurred before the maximum discharge of the season, increasing from 5 and 14 µmol/L. Dissolved Fe concentrations measured in the Råne River were slightly higher than in the Kalix River. Particulate Fe increased later, compared to the DFe, with values ranging from 4 to 20 µmol/L.

Riverine Fe input varies throughout the year and influences the Fe distribution along the estuaries and in the Bothnian Bay. The DFe concentration in the Kalix and Råne estuaries decreased with increasing salinities towards the open Bothnian Bay (Figs. 4, 5, Table 3). At most stations, the DFe concentration also decreased with depths as salinity increased. During spring flood, DFe in the Kalix estuary varied between 18.7 and 1.4 µmol/L. In the Råne estuary, the DFe concentration varied between 1.7 and 16.3 µmol/L (Fig. 5) with the lowest concentrations at depths of 10 m, where the salinities were comparably high. During late spring flood, the DFe concentration was slightly lower, but the decrease in DFe with depths was less distinct (6.4–14 µmol/L). Within the Bothnian Bay at salinities around 3 g/kg, the DFe concentration ranged from 0.1 to 0.8 µmol/L with little variation in depth (Fig. 6). The highest concentrations occurred at station A5 in June. Along both estuaries, the depths profiles suggest decreasing PFe concentrations from land to sea, but the trend was not as clear as in the dissolved fraction. In general, the PFe concentration decreased with depths. In the Kalix estuary, the PFe concentration ranged from 0.4 to 5.8 µmol/L during the spring flood. In the Råne estuary, the measured PFe concentration ranged from 0.4 to 6.5 µmol/L, whereas station R1 showed exceptional high PFe concentrations of 15.5 µmol/L. Particulate Fe in the open Bothnian Bay showed little variation between 0.1 and 0.7 µmol/L, whereas the highest concentrations occurred at station A5 during June (Fig. 6).

All Fe-isotope compositions in the particulate and the dissolved phase are relative to the reference material IRMM-14. Our data fall within Fe-isotope ratios described for the boreal and arctic regions [Dδ^{56}Fe: −1.2 to +1.8‰; Pδ^{56}Fe: −1.0 to +0.6‰; (Ilina et al. 2013; Escoube et al. 2015; Zhang et al. 2015; Opfergelt et al. 2017)]. Within the rivers, the Dδ^{56}Fe values varied between +0.47±0.10 and +0.59±0.05‰ in Kalix River and between +0.48±0.05 and +0.62±0.04‰ in Råne River (Fig. 3). The Pδ^{56}Fe values ranged from +0.24±0.10 to −0.06±0.08 in Kalix River and from +0.30±0.06 to −0.07±0.15‰ in Råne River. The DFe-isotope composition was at all times higher than the PFe-isotope values. The Dδ^{56}Fe composition showed small variations during the season, while the Pδ^{56}Fe composition, in both rivers, was more negative during spring flood. Between the two phases, a difference of minimum 0.3‰ points and a maximum of about 0.7‰ points were measured. There was a significant difference of 0.40‰ in the results for DFe (average 0.54‰; SD = 0.05‰) and PFe (average 0.07‰; SD = 0.12‰); $p < 0.001$, $n = 30$.

During spring flood, the DFe in the Kalix and Råne estuaries showed positive δ^{56}Fe values, which varied from +0.11±0.07 to +0.48±0.03‰ and from +0.32±0.13‰ to +0.49±0.04‰, respectively (Figs. 4, 5). Overall the transect profiles showed little variation with depths, the most distinct change occurs in the Kalix estuary between 5 and 10 m depth, with a shift from +0.40 to +0.16‰ (K3) and from +0.48 to +0.11‰ (K4) during late spring flood. The Fe-isotope composition of PFe showed negative values on
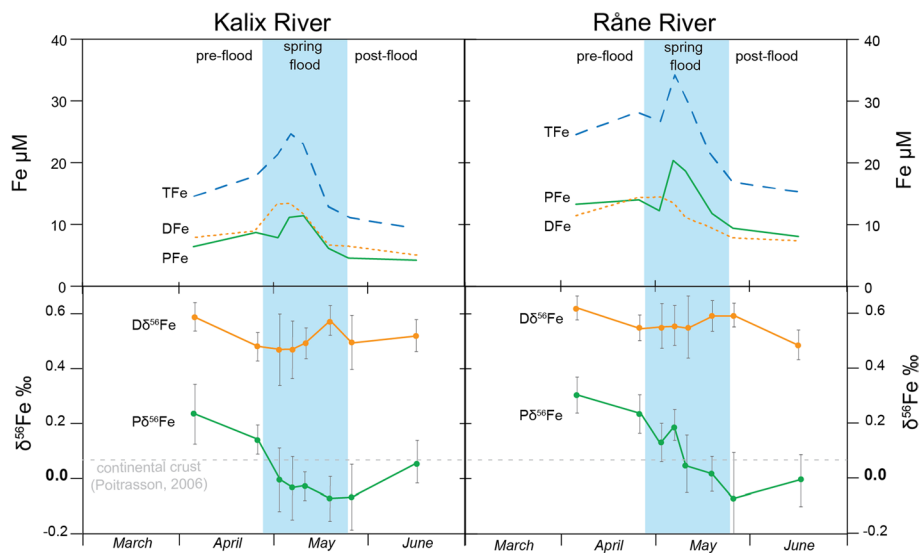
Fig. 3 Variation in Fe concentration and Fe-isotope composition in Kalix (left) and Råne River (right). The total Fe (TFe) concentration is calculated as the sum of DFe and PFe. The shaded area indicates the spring flood. Fe-isotopes are displayed as δ^{56}Fe relative to the IRMM-14 standard material. The errors are presented as 2SD

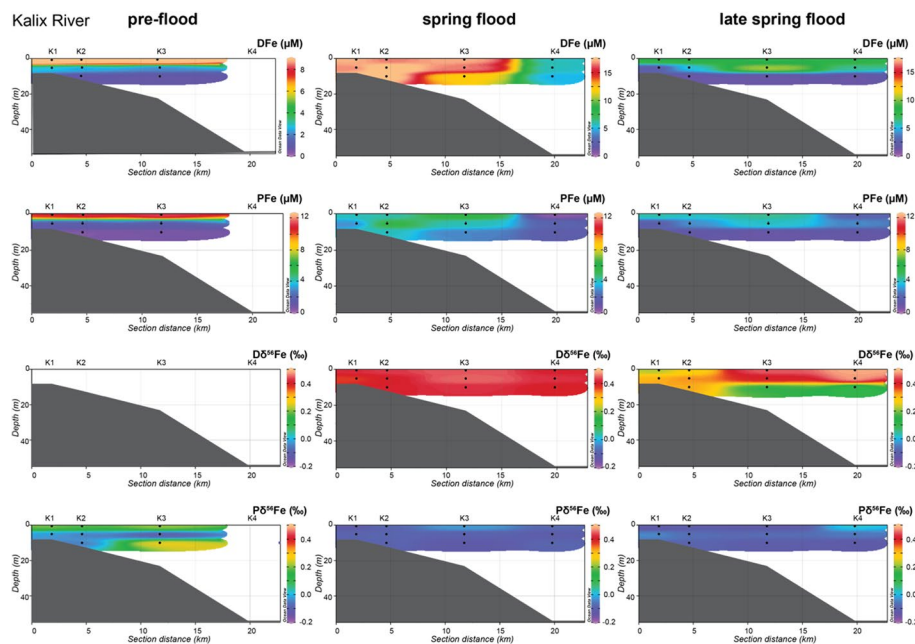**Fig. 4** Kalix estuary concentration transects for DFe (first row) and PFe (second row), as well as the Dδ^{56}Fe (third row) and Pδ^{56}Fe (fourth row) isotope composition. The stations were sampled during pre-flood, spring flood and late spring flood. The Ocean Data View program, version 4.7.10, was used to generate the transects (Schlitzer, R., Ocean Data View, http://odv.awi.de, 2018)

Fig. 5 Råne estuary concentration transects for DFe (first row) and PFe (second row), as well as the $D\delta^{56}Fe$ (third row) and $P\delta^{56}Fe$ (fourth row) isotope composition. The stations were sampled during pre-flood, spring flood and late spring flood. The Ocean Data View program, version 4.7.10, was used to generate the transects (Schlitzer, R., Ocean Data View, http://odv.awi.de, 2018)

the average and little variation with depths. Within the Kalix estuary, the $\delta^{56}Fe$ of PFe ranged from -0.13 ± 0.04 to $+0.02 \pm 0.09‰$. The $P\delta^{56}Fe$ in the Råne estuary tended to be slightly more positive and ranged from -0.07 ± 0.06 to $+0.09 \pm 0.05‰$. The $P\delta^{56}Fe$ within the Bothnian Bay showed little variation with an average of $+0.07 \pm 0.04‰$. There was a significant difference of 0.44‰ in the results for DFe (average 0.39‰; SD = 0.09‰) and for PFe (average $-0.05‰$; SD = 0.05‰); $t(41) = 2.59$, $p = 0.011$. Escoube et al. (2009) reported a difference between the two phases of 0.50‰.

4.2 Pre-flood and Post-flood

During pre-flood, discharge in the Kalix River is four to five times higher than in the Råne River. During post-flood on the other hand, the discharge of the Kalix River is about 23 times higher, due to the delayed snowmelt from the mountains in the catchment of the Kalix River (Fig. 2). The salinity in the estuaries during pre-flood varied between 0 and 2.6 g/kg (ESM_1 and _2), whereas just the surface water samples had salinities around 0 g/kg, the deeper samples had values between 1.7 and 2.6 g/kg. During post-flood, the water column in the Råne estuary (R2) was well mixed and showed an average salinity of 2.4 g/kg (ESM_1 and _2). The water column in the Bothnian Bay was well mixed with an average salinity of 3.2 g/kg. Dissolved OC concentrations were lowest in the rivers and estuaries during base flow conditions (242–552 μmol/L) (ESM_2). During pre-flood, the DOC concentrations in the Kalix estuary were lowest in the surface samples (293–303 μmol/L), and values increased with depths to 415 μmol/L. In the Råne estuary, DOC concentrations

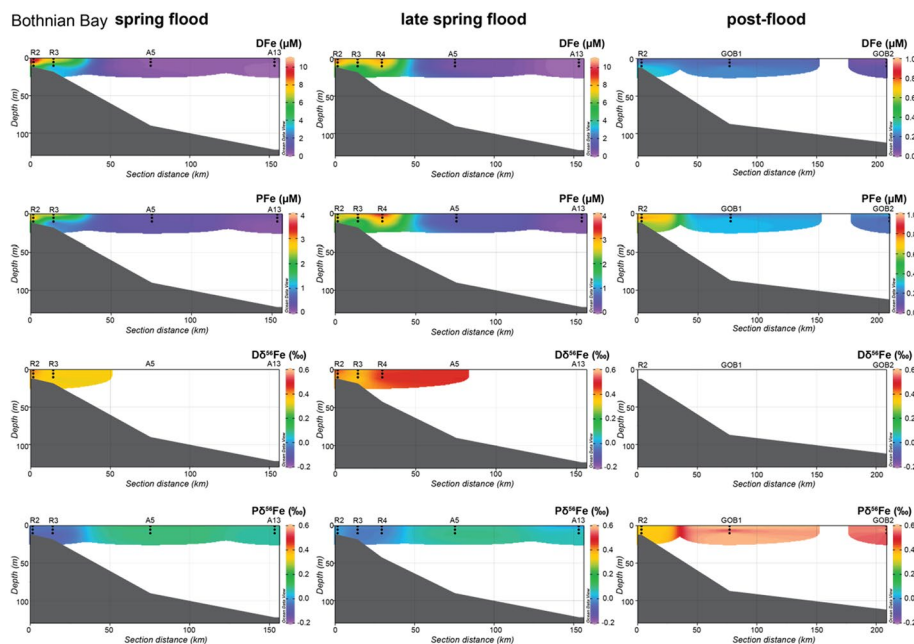**Fig. 6** Bothnian Bay concentration transects for DFe (first row) and PFe (second row), as well as the Dδ⁵⁶Fe (third row) and Pδ⁵⁶Fe (fourth row) isotope composition. The stations were sampled during spring flood and late spring flood and post-flood. For reference data, the transects start at station R2 in the Råne estuary. The Ocean Data View program, version 4.7.10, was used to generate the transects (Schlitzer, R., Ocean Data View, http://odv.awi.de, 2018)

at the water surface were higher (425–469 μmol/L) compared to the deeper waters (328 μmol/L) (ESM_2), the concentrations were similar during pre- and post-flood. Within the Bothnian Bay, the DOC varied between 117 and 393 μmol/L, with decreasing concentrations southwards. The DOC in these profiles increased with depth (ESM_2, Fig. S5).

During pre-flood, the DFe concentration varied between 0.2 and 13.2 μmol/L for both estuaries (Figs. 4, 5). The surface samples had very high concentrations (average 8.5 μmol/L) compared to the underlying water column (average 1.3 μmol/L). During post-flood, the DFe concentrations in the Råne estuary showed little variation with an average of 0.2 μmol/L (Fig. 6). The concentrations in the Bothnian Bay showed little variation around 0.1 μmol/L (Fig. 6). The surface waters sampled during pre-flood showed very high PFe concentrations (up to 13.3 μmol/L) values compared to the underlying water (on average 0.8 μmol/L). During post-flood, the PFe concentration in the Råne estuary ranged from 0.5 to 0.9 μmol/L. Samples from the Bothnian Bay after spring flood showed little variation between 0.1 and 0.3 μmol/L.

No dissolved Fe-isotope data are available for pre- and post-flood. The δ^{56}Fe composition of the PFe in the estuaries showed no clear trend during pre-flood (Figs. 4, 5). In the Kalix estuary, the Pδ^{56}Fe ranged from -0.09 ± 0.09 to $+0.21 \pm 0.07$‰, whereas just the surface water samples had a positive Fe-isotope composition. In the Råne estuary, the Pδ^{56}Fe ranged from $+0.02 \pm 0.05$ to $+0.14 \pm 0.05$‰ pre-flood and from $+0.32 \pm 0.06$ to $+0.38 \pm 0.07$‰ post-flood conditions. Within the Bothnian Bay during post-flood, the Pδ^{56}Fe composition ranged from $+0.48 \pm 0.11$ to $+0.67 \pm 0.15$‰.

5 Discussion

5.1 Temporal Variations of Fe

Seasonal dynamics in the boreal region suggest varying hydro-geological pathways throughout the year (Dahlqvist et al. 2007; Rosenberg and Schroth 2017). During pre-flood, low Fe and DOC concentrations, as well as high pH values, indicate groundwater as source for riverine input (Dahlqvist et al. 2007; Wortberg et al. 2017). In boreal regions, up to 2/3 of the annual discharge is transported during the spring flood (Pontér et al. 1990; Lidman et al. 2011). Increased discharge has a significant influence on the chemical composition of rivers, estuaries and the open sea. During spring flood, increasing DOC, Fe and decreasing pH suggest the inflow from organic-rich soil layers into the rivers (Seibert et al. 2009; Ledesma et al. 2015; Ingri et al. 2018). The riparian zone and its organic-rich soil layers are the main source for the increased DOC and Fe in subarctic, boreal forest rivers during the snow melt and the associated spring flood (Laudon and Bishop 1999; Bishop et al. 2004; Grabs et al. 2012). Recently, the flushing of the upper soil horizons in the catchment of the Kalix River has been validated with the use of the Rb/Sr ratio and Sr-isotope ratio by Wortberg et al. (2017). Our data show a clear correlation between the $P\delta^{56}Fe$ composition and the Rb/Sr ratio ($R^2 = 0.75$), with positive $P\delta^{56}Fe$ values corresponding with low Rb/Sr ratios, whereas a negative $P\delta^{56}Fe$ composition corresponds with the high Rb/Sr ratio—the identified flushing component. This correlation implies that the origin of a negative $\delta^{56}Fe$ composition is lying within the upper soil layers, available due to flushing events. The decrease in $P\delta^{56}Fe$ values from +0.24 to −0.06‰ in the Kalix River and from +.30 to −0.07‰ in the Råne River reflects the changing hydro-geological pathways between pre-flood and spring flood for PFe. The $D\delta^{56}Fe$ composition, on the other hand, is almost stable with an average composition of +0.53±0.05‰ throughout pre-flood, spring flood and post-flood, indicating no or little variation of the DFe source.

In boreal regions, Fe is transported in two primary forms in the rivers: Fe-OC complexes and Fe (oxy)hydroxides (Ilina et al. 2013; Neubauer et al. 2013; Sundman et al. 2014). In arctic and subarctic rivers, the high DOC concentration leads to the building of organo-mineral colloidal status for most metals, i.e. Fe (Pokrovsky et al. 2010; Schroth et al. 2011; Ingri et al. 2018). Organic carbon can stabilize Fe aggregates during transport (Kritzberg et al. 2014; Herzog et al. 2017). Salinity-induced aggregation experiments in both rivers resulted in an aggregated phase dominated by Fe(oxy)hydroxides with a lower Fe-isotope composition than the remaining suspended phase, with a higher amount of Fe-OM (Herzog et al. 2019). Therefore, we assume that DFe is dominated by Fe-OM complexes with positive Fe-isotope values, while PFe seems to be dominated by Fe(oxy)hydroxides with lower $\delta^{56}Fe$. Evidence suggests that the decrease in $P\delta^{56}Fe$ is caused by the input of negative Fe-OC complexes from organic-rich surface soils, flushed during spring flood. The comparable heavier values during pre- and post-flood origin from Fe(oxy)hydroxides precipitated from anoxic groundwaters with high amounts of dissolved Fe(II) concentrations (Neubauer et al. 2013). Boreal first-order streams have mainly Fe-OC complexes, where the Fe occurs in the reduced Fe(II) or a mixed Fe(II)/Fe(III) oxidation states (Emmenegger et al. 1998; Rose and Waite 2003; Sundman et al. 2013), the higher-order streams consist of Fe-OC complexes and nanoparticulate Fe(oxy)hydroxides, which aggregate and can be found in the > 0.22 μm fraction (Neubauer et al. 2013). With the decreasing amount of Fe-OC complexes, the amount of Fe(oxy)hydroxides with Fe(III) increases (Lofts et al. 2008; Neubauer et al. 2013).

Summarizing, we suggest that the DFe reaching the estuaries has a relatively stable δ^{56}Fe ($+0.53 \pm 0.05‰$) throughout the season, whereas the PFe reaching the estuaries is mainly Fe(oxy)hydroxides with a lower δ^{56}Fe during pre- and post-flood and a negative δ^{56}Fe signal during spring flood, caused by Fe-OC complexes from the riparian zone.

5.2 Fe in Low Salinity Mixing

The mixing of freshwater and seawater influences the salinity in the estuaries (Dyer 1973). During spring flood, the salinity within the estuaries is generally lower than during pre- and post-flood, due to the increased input of freshwater. The temporal and spatial measurements of salinity within the estuaries and the Bothnian Bay showed a fast-changing and responding system (ESM_2, Figs. S3 to 5). During spring flood, salinity measurements showed, (1) at peak discharge the estuaries are freshwater dominated; (2) the influence of freshwater vanishes within 2 weeks; (3) peak discharge can be traced out to the open Bothnian Bay. During pre-flood, salinity measurements show a layering in the Kalix and Råne estuaries (ESM_2, Figs. S3 and 4), the high salinities in 5 and 10 m depths suggest seawater, with generally higher salinities, are the primary influencer of the salinity in these areas. The low surface salinities might be caused by the ice on top of the water column. By drilling into the ice, the ice melts and dilutes the surface water. Salinity has a significant effect on the Fe and DOC interaction and concentration in the estuaries (Boyle et al. 1974; Holliday and Liss 1976). During spring flood, we observed about 50% removal of DOC along the estuaries, which is in accordance with data found for the Bothnian Bay and to other authors for the arctic region (Alling et al. 2010; Letscher et al. 2011; Deutsch et al. 2012).

During spring flood, Fe is transported out to the Bothnian Bay in a freshwater layer on top of the denser saltwater, which reaches as far as station K3 (Fig. 4). While the Bothnian Bay (A5 and A13) shows constant Fe values during spring flood, and during the late spring flood the freshwater input reached as far as station A5, where Fe concentration increased compared to earlier in the year (Fig. 6). Both DFe and PFe concentrations showed a non-conservative behaviour in the Kalix and Råne estuary, which has been found in other estuaries before (Boyle et al. 1977; Sholkovitz et al. 1978; Gustafsson et al. 2000). Dissolved Fe often contains a significant amount of Fe colloids (Schroth et al. 2011; Pokrovsky et al. 2012; Ilina et al. 2013; Conrad et al. 2019). The destabilisation of Fe-rich colloids and particles by seawater cations are one of the major factors for the flocculation (Mosley et al. 2003; Gerringa et al. 2007; Escoube et al. 2009). These flocculates might sink to the surface sediment or might be transported out of the estuaries (Daneshvar 2015). The amount of Fe flocculating at a certain salinity can be calculated. The flocculation factor F represents the fraction of DFe, which is removed by colloidal flocculation, with 1 equals 100% removal of DFe (Boyle et al. 1974; Escoube et al. 2009). The flocculation factor is calculated using two system end members, DFe and the salinity (S) of each sample. The samples R1a_05 (16.3 µmol/L DFe) and K1a_05 (17.3 µmol/L) are defined as the river end members, as they have relatively high Fe values and low salinity (<0.02 g kg^{-1}). The seawater end member should have less than 1% of the initial Fe concentration, we defined sample A13b_05 (0.1 µmol/L; 3 g kg^{-1}), as it showed the highest salinity concentration.

$$F = 1 - \left(\frac{\text{Fe}_{\text{SW}}}{\text{Fe}_{\text{RW}}} + \frac{\text{Fe}_{\text{S}} - \text{Fe}_{\text{SW}}}{\text{Fe}_{\text{RW}}} * \frac{1}{1 - S/35} \right)$$

The flocculation factor was calculated for the spring flood estuary data (Fig. 7), about 75% of the DFe flocculated at salinities below 1 g/kg and about 90% at salinities below 3 g/

kg. In comparison, Escoube et al. (2009) showed removal of DFe by colloidal flocculation of 50% below a salinity of 5 g/kg in the North River, which increased to 70% until a salinity of 10 g/kg. At salinities > 10 g/kg, the flocculation is stable between 70 and 80%. Our values indicate a higher removal of DFe at lower salinities in the estuaries compared to the North River. Earlier studies have suggested major removal of Fe between salinities of 5–15 g/kg in the Mullica estuary (USA) and the Amazonas and Para River (Brasil) (Boyle et al. 1974; Sholkovitz et al. 1978). Within boreal estuaries in Finland, significant removal at salinities below 2 g/kg was observed (Asmala et al. 2014). Increasing pH along the estuaries can affect the flocculation and precipitation of Fe oxides and hydroxides. At pH values below 6.5, the oxidation rate normally is low, while at higher pH values [e.g. 7.4–8.6; (Daneshvar 2015)] Fe oxides precipitate as hydrated ferric oxides. In both the Kalix and Råne estuaries, we observed an increase of pH from 6.5 to 7.4 between May and June 2013, which would increase the possibility to form solid-phase ferric iron oxides or hydroxides within the estuaries (Daneshvar 2015). Furthermore, the stability of Fe colloids and particles depends on their composition. The relationship between Fe and OC controls the stability of Fe colloids and aggregates during estuarine mixing and is highly dependent

Fig. 7 Flocculation factor of Fe and δ^{56}Fe versus salinity for Kalix and Råne estuaries during spring flood. The flocculation factor is calculated after Escoube et al. 2009 and for comparison their flocculation trend for the North River, Massachusetts, is displayed in grey in the upper panel. Open symbols display the particulate phase, while filled symbols display the dissolved phase. The error for δ^{56}Fe is presented as 2SD
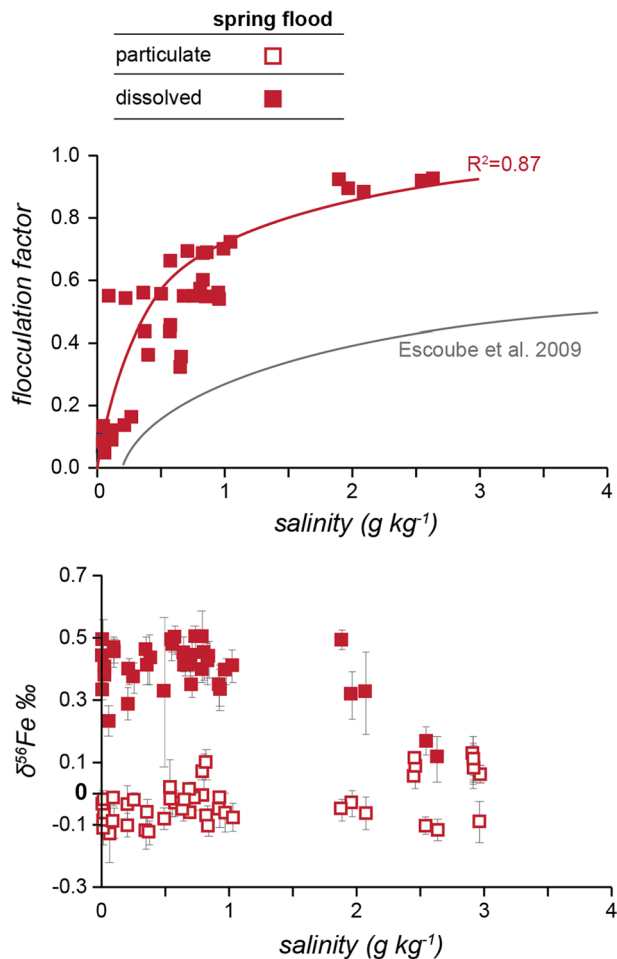
on the initial Fe:OC ratio (Asmala et al. 2014; Kritzberg et al. 2014; Jilbert et al. 2017). The aggregates and flocculates are removed from the water column by gravitational settling. Small, and therefore light, flocculates might remain suspended in the estuarine waters and travel out to the open sea. Lower total Fe concentrations in the open Bothnian Bay (A5) compared to the estuaries indicate that more Fe is scavenged out between station A5 and the estuaries.

The DFe concentrations in the estuaries during pre- and post-flood are much lower than during spring flood. The only exceptions are the surface waters, which showed elevated DFe concentrations during pre-flood. Studies of DFe and PFe in sea ice showed that the two Fe phases are enriched in the newly built ice (Lannuzel et al. 2010; Janssens et al. 2016). Drilling through the ice and accompanied ice melting might have caused the high DFe and PFe concentrations in the surface waters. Contamination of the water profile by sediment, which got redistributed to the water column, might cause the extreme PFe concentrations at station R1 during late spring flood.

Within both estuaries, we could observe the same two groups of Fe-isotopes that were observed in their rivers during spring flood (Fig. 7). In our study, DFe has a positive Fe-isotope composition from +0.11 to +0.49‰, within the range of earlier studies, which showed Fe-isotope compositions of various rivers between −1.2 and +1.8‰ (Ilina et al. 2013; Escoube et al. 2015; Zhang et al. 2015; Opfergelt et al. 2017). The PFe phase on the other hand shows lower and mostly negative Fe-isotope values (−0.13 to 0.09‰) comparable to published values in the range of −0.87 to +0.40‰ (Ingri et al. 2006; Ilina et al. 2016; Cheng et al. 2017; Opfergelt et al. 2017). The Fe-isotope signal in both fractions is stable during spring flood, suggesting that the source of the signal is available over a longer period. The particles formed during spring flood in the organic-rich soils are transported along the river through the river mouth into the estuaries. Therefore, in contrast to the Fe concentrations, the Fe-isotope compositions are stable along the salinity gradient. Within the Bothnian Bay, PFe-isotope values are slightly heavier than in the estuaries. We could not detect the negative Fe-isotope signal in the Bothnian Bay. Hence, the negative particles might be removed from the water column during estuarine mixing. The driver for the removal could be the different surface properties of the Fe-OC and Fe(oxy)hydroxide aggregates, which lead to different flocculation behaviours along the estuaries (Gustafsson et al. 2000).

Particulate Fe-isotope values during pre- and post-flood in the rivers, estuaries and the Bothnian Bay are generally heavier compared to values during spring flood. During pre-flood, the estuaries show values around +0.2‰, while during post-flood, the measured values are higher around +0.4‰. Suggesting that PFe delivers positive Fe-isotope values during base flow conditions in contrast to the spring flood. The post-flood PFe-isotope values in the Bothnian Bay are as high as +0.6‰ exceeding values found during earlier research [+0.1 to +0.2‰, (Gelting 2009)].

6 Conclusions

First of all, this study shows the stability of a natural system over decades. Earlier research in the Kalix River [since 1982, e.g. (Pontér et al. 1990; Ingri 1996)] showed similar behaviour of the Fe concentration and Fe-isotopes. The annual spring flood with the accompanying features of increasing Fe concentrations and decreasing Fe-isotope compositions is a regular and periodic event influencing the water geochemistry. Our data set complements

earlier research with the dissolved phase, as well as additional data how the Fe-isotope signal is transported along the estuaries into the Bothnian Bay.

1. The merged Fe-isotope signal of a subarctic, forest dominated catchment can be divided into the dissolved and particulate phase. Within the rivers and estuaries, we found positive Fe-isotopes in the dissolved phase and negative Fe-isotopes in the particulate phase during spring discharge.
2. The correlation between different chemical parameters Fe and DOC allows us to conclude that the Fe-isotope composition during spring flood is evolving in the organic-rich soil layers of first-order streams. Therefore, the lighter Fe-isotope signal is correlated to the organic-rich soil layers of the riparian zones. During pre- and post-flood, PFe has a positive Fe-isotope signal. This shows that Fe has different origins throughout the season.
3. Salt-induced flocculation on a small salinity range, up to 1 g/kg, is removing about 80% of the dissolved and particulate Fe during estuarine mixing. Increasing salinity and pH lead to the formation of colloids and particles, which sediment due to small changes in ionic strength. Within the low salinity estuaries, salt-induced flocculation is removing about 90% of the dissolved and particulate Fe. This major flocculation at low salinities might cause an underestimation of riverine Fe flux. Within the estuarine mixing zone, no Fe-isotope fractionation was observed. During spring flood, the Fe-isotope signal is constant along the estuaries, which excludes fractionation processes for example by oxidation.
4. The Fe-isotope signal within the Bothnian Bay was positive showing that different surface properties of Fe-OC and Fe(oxy)hydroxide aggregates lead to the flocculation of negative Fe aggregates.

References

Alling V, Sanchez-Garcia L, Porcelli D, Pugach S, Vonk JE, Van Dongen B, Mörth CM, Anderson LG, Sokolov A, Andersson P, Humborg C, Semiletov I, Gustafsson Ö (2010) Nonconservative behavior of dissolved organic carbon across the Laptev and East Siberian seas. Global Biogeochem Cycles 24:1–15. https://doi.org/10.1029/2010GB003834

Asmala E, Bowers DG, Autio R, Kaartokallio H, Thomas DN (2014) Qualitative changes of riverine dissolved organic matter at low salinities due to flocculation. J Geophys Res Biogeosci 119:1919–1933. https://doi.org/10.1002/2013JG002433

Bauer S, Blomqvist S, Ingri J (2018) Distribution of dissolved and suspended particulate molybdenum, vanadium, and tungsten in the Baltic Sea. Mar Chem 196:135–147. https://doi.org/10.1016/j.marchem.2017.08.010

Baxter DC, Rodushkin I, Engström E, Malinovsky D (2006) Revised exponential model for mass bias correction using an internal standard for isotope abundance ratio measurements by multi-collector inductively coupled plasma mass spectrometry. J Anal At Spectrom 21:427. https://doi.org/10.1039/b517457k

Bishop K, Seibert J, Köhler S, Laudon H (2004) Resolving the Double Paradox of rapidly mobilized old water highly variable responses in runoff chemistry. Hydrol Process 18:185–189. https://doi.org/10.1002/hyp.5209

Boyle E, Collier R, Dengler AT (1974) On the chemical mass-balance in estuaries. Geochim Cosmochim Acta 38:1719–1728. https://doi.org/10.1016/0016-7037(74)90188-4

Boyle EA, Edmond JM, Sholkovitz ER (1977) The mechanism of iron removal in estuaries. Geochim Cosmochim Acta 41:1313–1324. https://doi.org/10.1016/0016-7037(77)90075-8

Brodie CR, Leng MJ, Casford JSL, Kendrick CP, Lloyd JM, Yongqiang Z, Bird MI (2011) Evidence for bias in C and N concentrations and δ13C composition of terrestrial and aquatic organic materials due to pre-analysis acid preparation methods. Chem Geol 282:67–83. https://doi.org/10.1016/j.chemgeo.2011.01.007

Cheng F, Liu S, Yin Y, Zhang Y, Zhao Q, Dong S (2017) Identifying trace metal distribution and occurrence in sediments, inundated soils, and non-flooded soils of a reservoir catchment using Self-Organizing Maps, an artificial neural network method. Environ Sci Pollut Res 24:19992–20004. https://doi.org/10.1007/s11356-017-9559-3

Conrad S (2019) Iron isotopes in aquatic systems. Luleå University of Technology, Luleå

Conrad S, Ingri J, Gelting J, Nordblad F, Engström E, Rodushkin I, Andersson PS, Porcelli D, Gustafsson Ö, Semiletov I, Öhlander B (2019) Distribution of Fe isotopes in particles and colloids in the salinity gradient along the Lena River plume, Laptev Sea. Biogeosci Discuss 16:1–27. https://doi.org/10.5194/bg-2018-181

Conway TM, John SG (2015) The cycling of iron, zinc and cadmium in the North East Pacific Ocean—insights from stable isotopes. Geochim Cosmochim Acta 164:262–283. https://doi.org/10.1016/j.gca.2015.05.023

Cutter G, Andersson P, Codispoti L, Croot P, Francois R, Lohan M, Obata H, Rutgers M (2010) Sampling and sample-handling protocols for GEOTRACES cruises. http://www.geotraces.org/library/geotraces-policies/170-sampling-and-sample-handling-protocols-for-geotraces-cruises, pp 1–238 http://www.geotraces.org/science/intercalibration/222-sampling-and-sample-handling-protocols-for-geotraces-cruises

Dahlqvist R, Andersson K, Ingri J, Larsson T, Stolpe B, Turner D (2007) Temporal variations of colloidal carrier phases and associated trace elements in a boreal river. Geochim Cosmochim Acta 71:5339–5354. https://doi.org/10.1016/j.gca.2007.09.016

Daneshvar E (2015) Dissolved iron behavior in the ravenglass estuary waters, an implication on the early diagenesis. Univers J Geosci 2015:1–12. https://doi.org/10.13189/ujg.2015.030101

Dauphas N, Rouxel O (2006) Mass spectrometry and natural variations of iron isotopes. Mass Spectrom Rev 25:515–520. https://doi.org/10.1002/mas.20078

Dauphas N, John SG, Rouxel O (2017) Iron isotope systematics. Rev Miner Geochem 82:415–510. https://doi.org/10.2138/rmg.2017.82.11

Deutsch B, Alling V, Humborg C, Korth F, Mörth CM (2012) Tracing inputs of terrestrial high molecular weight dissolved organic matter within the Baltic Sea ecosystem. Biogeosciences 9:4465–4475. https://doi.org/10.5194/bg-9-4465-2012

Dos Santos Pinheiro GM, Poitrasson F, Sondag F, Cochonneau G, Vieira LC (2014) Contrasting iron isotopic compositions in river suspended particulate matter: the Negro and the Amazon annual river cycles. Earth Planet Sci Lett 394:168–178. https://doi.org/10.1016/j.epsl.2014.03.006

Dyer KR (1973) Estuaries—a physical introduction, 2nd edn. Wiley, Chichester

Eckert JM, Sholkovitz ER (1976) The flocculation of iron, aluminum and humates from river water by electrolytes. Geochim Cosmochim Acta 40:847–848

Emmenegger L, Whitney King D, Sigg L, Sulzberger B (1998) Oxidation kinetics of Fe(II) in a eutrophic swiss lake. Environ Sci Technol 32:2990–2996. https://doi.org/10.1021/es980207g

Escoube R, Rouxel OJ, Sholkovitz E, Donard OFX (2009) Iron isotope systematics in estuaries: the case of North River, Massachusetts (USA). Geochim Cosmochim Acta 73:4045–4059. https://doi.org/10.1016/j.gca.2009.04.026

Escoube R, Rouxel OJ, Pokrovsky OS, Schroth A, Max Holmes R, Donard OFX (2015) Iron isotope systematics in Arctic rivers. Comptes Rendus Geosci 347:377–385. https://doi.org/10.1016/j.crte.2015.04.005

Eusterhues K, Wagner FE, Ha W, Hanzlik M, Knicker H, Totsche KU, Ko I, Schwertmann U (2008) Characterization of ferrihydrite-soil organic matter coprecipitates by X-ray diffraction and Mo # ssbauer Spectroscopy characterization of ferrihydrite-soil organic matter coprecipitates by X-ray diffraction and Mo spectroscopy. Environ Sci Technol 42:7891–7897. https://doi.org/10.1021/es800881w

Gelting J (2009) Speciation of trace metals in the Baltic sea with focus on the euphotic zone. Luleå University of Technology, Luleå

Gerringa LJA, Rijkenberg MJA, Wolterbeek HT, Verburg TG, Boye M, de Baar HJW (2007) Kinetic study reveals weak Fe-binding ligand, which affects the solubility of Fe in the Scheldt estuary. Mar Chem 103:30–45. https://doi.org/10.1016/j.marchem.2006.06.002

Grabs T, Bishop K, Laudon H, Lyon SW, Seibert J (2012) Riparian zone hydrology and soil water total organic carbon (TOC): implications for spatial variability and upscaling of lateral riparian TOC exports. Biogeosciences 9:3901–3916. https://doi.org/10.5194/bg-9-3901-2012

Gustafsson Ö, Widerlund A, Andersson PS, Ingri J, Roos P, Ledin A (2000) Colloid dynamics and transport of major elements through a boreal river—Brackish bay mixing zone. Mar Chem 71:1–21. https://doi.org/10.1016/S0304-4203(00)00035-9

Haei M, Öquist MG, Buffam I, Ågren A, Blomkvist P, Bishop K, Löfvenius MO, Laudon H (2010) Cold winter soils enhance dissolved organic carbon concentrations in soil and stream water. Geophys Res Lett 37:1–5. https://doi.org/10.1029/2010GL042821

Herzog SD, Persson P, Kritzberg ES (2017) Salinity effects on iron speciation in boreal river waters. Environ Sci Technol 51:9747–9755. https://doi.org/10.1021/acs.est.7b02309

Herzog SD, Conrad S, Ingri J, Persson P, Kritzberg ES (2019) Spring flood induced shifts in Fe speciation and fate at increased salinity. Appl Geochem 109:104385. https://doi.org/10.1016/j.apgeochem.2019.104385

Holliday LM, Liss PS (1976) The behaviour of dissolved iron, manganese and zinc in the Beaulieu Estuary. S Engl Estuar Coast Mar Sci 4:349–353

Ilina SM, Poitrasson F, Lapitskiy SA, Alekhin YV (2013) Extreme iron isotope fractionation between different size colloids of boreal organic-rich waters. Geochim Cosmochim Acta 101:96–111. https://doi.org/10.1016/j.gca.2012.10.023

Ilina SM, Lapitskiy SA, Alekhin YV, Viers J, Benedetti M, Pokrovsky OS (2016) Speciation, size fractionation and transport of trace elements in the continuum soil water–mire–humic lake–river–large oligotrophic lake of a subarctic watershed. Aquat Geochem 22:65–95. https://doi.org/10.1007/s10498-015-9277-8

Ingri J (1996) Kalixälvens hydrogeokemi. Luleå University of Technology, Luleå

Ingri J, Widerlund A, Land M (2005) Geochemistry of major elements in a pristine boreal river system; hydrological compartments and flow paths. Aquat Geochem 11:57–88. https://doi.org/10.1007/s10498-004-2248-0

Ingri J, Malinovsky D, Rodushkin I, Baxter DC, Widerlund A, Andersson P, Gustafsson Ö, Forsling W, Öhlander B (2006) Iron isotope fractionation in river colloidal matter. Earth Planet Sci Lett 245:792–798. https://doi.org/10.1016/j.epsl.2006.03.031

Ingri J, Conrad S, Lidman F, Nordblad F, Engström E, Rodushkin I, Porcelli D (2018) Iron isotope pathways in the boreal landscape: role of the riparian zone. Geochim Cosmochim Acta 239:49–60. https://doi.org/10.1016/j.gca.2018.07.030

Janssens J, Meiners KM, Tison J-L, Dieckmann G, Delille B, Lannuzel D (2016) Incorporation of iron and organic matter into young Antarctic sea ice during its initial growth stages. Elem Sci Anthr 4:000123. https://doi.org/10.12952/journal.elementa.000123

Jilbert T, Asmala E, Schröder C, Tiihonen R, Myllykangas J-P, Virtasalo JJ, Kotilainen A, Peltola P, Ekholm P, Hietanen S (2017) Flocculation of dissolved organic matter controls the distribution of iron in boreal estuarine sediments. Biogeosci Discuss. https://doi.org/10.5194/bg-2017-181

Kautsky L, Kautsky N (2000) The baltic sea, including bothnian sea and bothnian bay. In: Sheppard CRC (ed) Seas at the millennium: an environmental evaluation, Chap 8, 1st edn. Elsevier Science Ltd, pp 121–133

Kavner A, Bonet F, Shahar A, Simon J, Young E (2005) The isotopic effects of electron transfer: an explanation for Fe isotope fractionation in nature. Geochim Cosmochim Acta 69:2971–2979. https://doi.org/10.1016/j.gca.2005.01.014

Knorr KH (2013) DOC-dynamics in a small headwater catchment as driven by redox fluctuations and hydrological flow paths—are DOC exports mediated by iron reduction/oxidation cycles? Biogeosciences 10:891–904. https://doi.org/10.5194/bg-10-891-2013

Krachler R, Krachler RF, von der Kammer F, Süphandag A, Jirsa F, Ayromlou S, Hofmann T, Keppler BK (2010) Relevance of peat-draining rivers for the riverine input of dissolved iron into the ocean. Sci Total Environ 408:2402–2408. https://doi.org/10.1016/j.scitotenv.2010.02.018

Kritzberg ES, Ekström SM (2012) Increasing iron concentrations in surface waters—a factor behind brown-ification? Biogeosciences 9:1465–1478. https://doi.org/10.5194/bg-9-1465-2012

Kritzberg ES, Villanueva AB, Jung M, Reader HE (2014) Importance of boreal rivers in providing iron to marine waters. PLoS ONE. https://doi.org/10.1371/journal.pone.0107500

Lalonde K, Mucci A, Ouellet A, Gélinas Y (2012) Preservation of organic matter in sediments promoted by iron. Nature 483:198–200. https://doi.org/10.1038/nature10855

Lannuzel D, Schoemann V, De Jong J, Pasquer B, Van Der Merwe P, Masson F, Tison JL, Bowie A (2010) Distribution of dissolved iron in Antarctic sea ice: spatial, seasonal, and inter-annual variability. J Geophys Res Biogeosci 115:1–13. https://doi.org/10.1029/2009JG001031

Laudon H, Bishop KH (1999) Quantifying sources of acid neutralisation capacity depression during spring flood episodes in Northern Sweden. Environ Pollut 105:427–435. https://doi.org/10.1016/S0269-7491(99)00036-6

Ledesma JLJ, Grabs T, Bishop KH, Schiff SL, Köhler SJ (2015) Potential for long-term transfer of dissolved organic carbon from riparian zones to streams in boreal catchments. Glob Chang Biol 21:2963–2979. https://doi.org/10.1111/gcb.12872

Letscher RT, Hansell DA, Kadko D (2011) Rapid removal of terrigenous dissolved organic carbon over the Eurasian shelves of the Arctic Ocean. Mar Chem 123:78–87. https://doi.org/10.1016/j.marchem.2010.10.002

Lidman F, Mörth CM, Björkvald L, Laudon H (2011) Selenium dynamics in boreal streams: the role of wetlands and changing groundwater tables. Environ Sci Technol 45:2677–2683. https://doi.org/10.1021/es102885z

Lofts S, Tipping E, Hamilton-Taylor J (2008) The chemical speciation of Fe(III) in freshwaters. Aquat Geochem 14:337–358. https://doi.org/10.1007/s10498-008-9040-5

Martin JH, Gordon RM, Fitzwater SE (1991) Iron limitation? Limnol Ocean 36:1793–1802. https://doi.org/10.4319/lo.1991.36.8.1793

Morel FMM, Price NM (2003) The biogeochemical cycles of trace metals. Science 80(300):944–948. https://doi.org/10.1126/science.1083545

Mosley LM, Hunter KA, Ducker WA (2003) Forces between colloid particles in natural waters. Environ Sci Technol 37:3303–3308. https://doi.org/10.1021/es026216d

Neubauer E, Schenkeveld WDC, Plathe KL, Rentenberger C, von der Kammer F, Kraemer SM, Hofmann T (2013) The influence of pH on iron speciation in podzol extracts: iron complexes with natural organic matter, and iron mineral nanoparticles. Sci Total Environ 461–462:108–116. https://doi.org/10.1016/j.scitotenv.2013.04.076

Ödman F, Ruth T, Pontér C (1999) Validation of a field filtration technique for characterization of suspended particulate matter from freshwater. Part I. Major elements. Appl Geochem 14:301–317. https://doi.org/10.1016/S0883-2927(98)00050-X

Opfergelt S, Williams HM, Cornelis JT, Guicharnaud RA, Georg RB, Siebert C, Gislason SR, Halliday AN, Burton KW (2017) Iron and silicon isotope behaviour accompanying weathering in Icelandic soils, and the implications for iron export from peatlands. Geochim Cosmochim Acta 217:273–291. https://doi.org/10.1016/j.gca.2017.08.033

Öquist MG, Laudon H (2008) Winter soil frost conditions in boreal forests control growing season soil CO_2 concentration and its atmospheric exchange. Glob Chang Biol 14:2839–2847. https://doi.org/10.1111/j.1365-2486.2008.01669.x

Peel MC, Finlayson BL, Mcmahon TA (2007) Updated world map of the Köppen–Geiger climate classification. Hydrol Earth Syst Sci 11:1633–1644

Poitrasson F, Cruz Vieira L, Seyler P, dos Santos Márcia, Pinheiro G, Santos Mulholland D, Bonnet MP, Martinez JM, Alcantara Lima B, Resende Boaventura G, Chmeleff JÔ, Dantas EL, Guyot JL, Mancini L, Martins Pimentel M, Ventura Santos R, Sondag F, Vauchel P (2014) Iron isotope composition of the bulk waters and sediments from the Amazon River Basin. Chem Geol 377:1–11. https://doi.org/10.1016/j.chemgeo.2014.03.019

Pokrovsky OS, Viers J, Shirokova LS, Shevchenko VP, Filipov AS, Dupré B (2010) Dissolved, suspended, and colloidal fluxes of organic carbon, major and trace elements in the Severnaya Dvina River and its tributary. Chem Geol 273:136–149. https://doi.org/10.1016/j.chemgeo.2010.02.018

Pokrovsky OS, Viers J, Dupré B, Chabaux F, Gaillardet J, Audry S, Prokushkin AS, Shirokova LS, Kirpotin SN, Lapitsky SA, Shevchenko VP (2012) Biogeochemistry of carbon, major and trace elements in watersheds of northern Eurasia drained to the Arctic Ocean: the change of fluxes, sources and mechanisms under the climate warming prospective. Comptes Rendus Geosci 344:663–677. https://doi.org/10.1016/j.crte.2012.08.003

Pontér C, Ingri J, Burman JO, Boström K (1990) Temporal variations in dissolved and suspended iron and manganese in the Kalix River, northern Sweden. Chem Geol 81:121–131. https://doi.org/10.1016/0009-2541(90)90042-6

Poulton SW, Raiswell R (2005) Chemical and physical characteristics of iron oxides in riverine and glacial meltwater sediments. Chem Geol 218:203–221. https://doi.org/10.1016/j.chemgeo.2005.01.007

Raiswell R, Canfield DE (2012) The iron biogeochemical cycle past and present. Geochem Perspect 1:1–220. https://doi.org/10.7185/geochempersp.1.1

Rodushkin I, Ruth T (1997) Determination of trace metals in estuarine and sea-water reference materials by high resolution inductively coupled plasma mass spectrometry. J Anal At Spectrom 12:1181–1185. https://doi.org/10.1039/a702486j

Rodushkin I, Nordlund P, Engström E, Baxter DC (2005) Improved multi-elemental analyses by inductively coupled plasma-sector field mass spectrometry through methane addition to the plasma. J Anal At Spectrom 20:1250–1255. https://doi.org/10.1039/b507886e

Rodushkin I, Engström E, Baxter DC (2010) Sources of contamination and remedial strategies in the multi-elemental trace analysis laboratory. Anal Bioanal Chem 396:365–377. https://doi.org/10.1007/s00216-009-3087-z

Rodushkin I, Pallavicini N, Engström E, Sörlin D, Öhlander B, Ingri J, Baxter DC (2016) Assessment of the natural variability of B, Cd, Cu, Fe, Pb, Sr, Tl and Zn concentrations and isotopic compositions in leaves, needles and mushrooms using single sample digestion and two-column matrix separation. J Anal At Spectrom 31:220–233. https://doi.org/10.1039/C5JA00274E

Rose AL, Waite TD (2003) Effect of dissolved natural organic matter on the kinetics of ferrous iron oxygenation in seawater. Environ Sci Technol 37:4877–4886. https://doi.org/10.1021/es034152g

Rosenberg BD, Schroth AW (2017) Coupling of reactive riverine phosphorus and iron species during hot transport moments: impacts of land cover and seasonality. Biogeochemistry 132:103–122. https://doi.org/10.1007/s10533-016-0290-9

Rouxel OJ, Auro M (2010) Iron isotope variations in coastal seawater determined by multicollector ICP-MS. Geostand Geoanal Res 34:135–144. https://doi.org/10.1111/j.1751-908X.2010.00063.x

Sarkkola S, Nieminen M, Koivusalo H, Laurén A, Kortelainen P, Mattsson T, Palviainen M, Piirainen S, Starr M, Finér L (2013) Iron concentrations are increasing in surface waters from forested headwater catchments in eastern Finland. Sci Total Environ 463–464:683–689. https://doi.org/10.1016/j.scitotenv.2013.06.072

Schroth AW, Crusius J, Chever F, Bostick BC, Rouxel OJ (2011) Glacial influence on the geochemistry of riverine iron fluxes to the Gulf of Alaska and effects of deglaciation. Geophys Res Lett 38:1–6. https://doi.org/10.1029/2011GL048367

Seibert J, Grabs T, Köhler S, Laudon H, Winterdahl M, Bishop K (2009) Linking soil- and stream-water chemistry based on a riparian flow-concentration integration model. Hydrol Earth Syst Sci 13:2287–2297. https://doi.org/10.5194/hess-13-2287-2009

Severmann S, Johnson CM, Beard BL, McManus J (2006) The effect of early diagenesis on the Fe isotope compositions of porewaters and authigenic minerals in continental margin sediments. Geochim Cosmochim Acta 70:2006–2022. https://doi.org/10.1016/J.GCA.2006.01.007

Shields MR, Bianchi TS, Gélinas Y, Allison MA, Twilley RR (2016) Enhanced terrestrial carbon preservation promoted by reactive iron in deltaic sediments. Geophys Res Lett 43:1149–1157. https://doi.org/10.1002/2015GL067388

Sholkovitz ER (1978) The flocculation of dissolved Fe, Mn, Al, Cu, Ni, Co and Cd during estuarine mixing. Earth Planet Sci Lett 41:77–86. https://doi.org/10.1016/0012-821X(78)90043-2

Sholkovitz ER, Boyle EA, Price NB (1978) The removal of dissolved humic acids and iron during estuarine mixing. Earth Planet Sci Lett 40:130–136. https://doi.org/10.1016/0012-821X(78)90082-1

SMHI (2018) Swedish meteorological and hydrological institute. https://www.smhi.se

Sundman A, Karlsson T, Persson P (2013) An experimental protocol for structural characterization of Fe in dilute natural waters. Environ Sci Technol 47:8557–8564. https://doi.org/10.1021/es304630a

Sundman A, Karlsson T, Laudon H, Persson P (2014) XAS study of iron speciation in soils and waters from a boreal catchment. Chem Geol 364:93–102. https://doi.org/10.1016/j.chemgeo.2013.11.023

Tagliabue A, Bowie AR, Boyd PW, Buck KN, Johnson KS, Saito MA (2017) The integral role of iron in ocean biogeochemistry. Nature 543:51–59. https://doi.org/10.1038/nature21058

Vihma T, Haapala J (2009) Geophysics of sea ice in the Baltic Sea: a review. Prog Oceanogr 80:129–148. https://doi.org/10.1016/j.pocean.2009.02.002

Wedepohl KH (1995) The composition of the continental crust. Geochim Cosmochim Acta 59:1217–1232. https://doi.org/10.1016/0016-7037(95)00038-2

Wells ML, Price NM, Bruland KW (1995) Iron chemistry in seawater and its relationship to phytoplankton: a workshop report. Mar Chem 48:157–182. https://doi.org/10.1016/0304-4203(94)00055-I

Wiederhold JG, Kraemer SM, Teutsch N, Borer PM, Halliday AN, Kretzschmar R (2006) Iron isotope frac-
    tionation during proton-promoted, ligand-controlled, and reductive dissolution of goethite. Environ Sci
    Technol 40:3787–3793. https://doi.org/10.1021/es052228y

Wortberg K, Conrad S, Andersson PS, Ingri J (2017) Strontium isotopes—a tracer for river suspended iron
    aggregates. Appl Geochem 79:85–90. https://doi.org/10.1016/j.apgeochem.2017.02.012

Wu B, Amelung W, Xing Y, Bol R, Berns AE (2018) Iron cycling and isotope fractionation in terrestrial
    ecosystems. Earth Sci Rev 190:323–352. https://doi.org/10.1016/j.earscirev.2018.12.012

Young ED, Galy AD, Naghara H (2002) Kinetic and equilibrium mass-dependent isotopic fractionation
    laws in nature and their geochemical and cosmochemical significance. Geochim Cosmochim Acta
    66:1095–1104

Zhang F, Zhu X, Yan B, Kendall B, Peng X, Li J, Algeo TJ, Romaniello S (2015) Oxygenation of a Cryo-
    genian ocean (Nanhua Basin, South China) revealed by pyrite Fe isotope compositions. Earth Planet
    Sci Lett 429:11–19. https://doi.org/10.1016/J.EPSL.2015.07.021

Affiliations

Sarah Conrad[1] · **Kathrin Wuttig[2,3]** · **Nils Jansen[2,4]** · **Ilia Rodushkin[5]** ·
Johan Ingri[1]

Kathrin Wuttig
kathrin.wuttig@utas.edu.au

Nils Jansen
dr.nils.jansen@gmail.com

Ilia Rodushkin
ilia.rodushkin@alsglobal.com

Johan Ingri
johan.ingri@ltu.se

[1]   Applied Geochemistry, Luleå University of Technology, 971 87 Luleå, Sweden

[2]   GEOMAR Helmholtz Centre for Ocean Research Kiel, Düsternbrooker Weg 20, 24105 Kiel,
      Germany

[3]   Antarctic Climate and Ecosystems Cooperative Research Centre, University of Tasmania, Private
      Bag 80, Hobart, TAS 7001, Australia

[4]   Institute for Marine and Antarctic Studies, University of Tasmania, Hobart, TAS, Australia

[5]   ALS Laboratory Group, ALS Scandinavia AB, Aurorum 10, 971 75 Luleå, Sweden